

Short-Range-Order Effects in Neutron Scattering from Heisenberg Paramagnets: Application to RbMnF_3

RAZA A. TAHIR-KHELI* AND DANIEL G. MCFADDEN†‡

Department of Physics, Temple University, Philadelphia, Pennsylvania 19122

(Received 27 October 1969)

We have computed the wave-vector-dependent frequency moments of the spectral line shape, $S(\mathbf{K}, \omega)$, of a Heisenberg paramagnet with isotropic exchange interaction of arbitrary range. The results are specialized to RbMnF_3 at $T = 3.5T_N$. Using the phenomenological representation of a two-parameter Gaussian diffusivity, the spectral line shape $S(\mathbf{K}, \omega)$ is constructed. The theoretical results are compared and found to be in satisfactory agreement with the experimental data of Windsor, Briggs, and Kestigian.

I. INTRODUCTION

SOME time ago, Van Hove¹ showed that the frequency and wave-vector distribution of the scattered neutron spectrum images the cooperative dynamical properties of the many-body scatterer. The scattered neutrons undergo two types of scattering: nuclear scattering and magnetic scattering. The former is caused by the interaction of the neutron with the nuclei of the scatterer through the intermediary of purely nuclear forces. For slow neutrons, the nuclear-scattering cross sections are typically of the order of magnitude of one barn. The magnetic scattering arises because the neutron has a finite magnetic moment which interacts with the magnetic moment of the atom. If the constituent atoms of the scatterer do not possess any effective magnetic moment density then clearly the latter type of scattering would be absent. However, for systems which are magnetic such a scattering is typically of the same order of magnitude as the nuclear scattering.²

Due to the rather distinct origins of the two types of scattering mentioned above, it is often possible to differentiate^{3,4} between the two. In any event, for present purposes we assume that such is indeed the case and address ourselves only to the study of some aspects of magnetic scattering.

The thermodynamics of interacting many spin systems is in general too complicated to be exactly soluble. Of the many approximate solutions which are known only the ones relating to low temperatures⁵⁻⁷ and to high temperatures⁸ are reliable. The dynamics of these systems (which is even more complicated than

the thermodynamics) is, of course, known even less reliably. At very low temperatures, where the system is well described in terms of quasi-independent Boson-like elementary excitations (i.e., spin waves), the frequency-wave-vector-dependent susceptibilities have recently been calculated to a high degree of precision.⁹ In the opposite temperature limit, i.e., $T \rightarrow \infty$, the situation is less satisfactory and except for some exact model calculations,¹⁰ only phenomenological analyses have thus far been carried out.¹¹⁻¹⁷

At the elevated temperatures assumed in Ref. 17, the system is almost completely random. As the temperature is lowered to finite values, the constituent spins of the magnetic system experience the presence of short-range order (SRO). The effects of SRO upon the spin dynamics (i.e., as exhibited by the frequency wave-vector dependent susceptibilities measured by inelastic neutron scattering experiments), however, have not been analyzed even in terms of the phenomenological concepts used for infinite temperature.¹⁵

For magnetic systems with strong exchange coupling, the neutron-scattering experiments are usually performed at temperatures not much higher than a few times their magnetic critical temperatures. Under these conditions, the presence of the SRO may be expected to make important contributions.¹⁸

* R. Silberglitt and A. B. Harris, Phys. Rev. **174**, 640 (1968).

¹⁰ A discussion of these exact "model" calculations is given by D. G. McFadden and R. A. Tahir-Kheli, Phys. Rev. (to be published).

¹¹ J. H. Van Vleck, Phys. Rev. **55**, 924 (1939).

¹² P. G. De Gennes, J. Phys. Chem. Solids **4**, 223 (1958); **6**, 43 (1958); also see *Magnetism*, edited by G. T. Rado and H. Suhl (Academic Press Inc., New York), Vol. 3, p. 115.

¹³ R. Kubo and K. Tomita, J. Phys. Soc. Japan **9**, 888 (1954).

¹⁴ M. F. Collins and W. Marshall, Proc. Phys. Soc. (London) **92**, 390 (1967).

¹⁵ W. Marshall and R. D. Lowde, Rept. Progr. Phys. **31**, 705 (1968).

¹⁶ T. H. Kwon and H. A. Gersch, Phys. Rev. **167**, 458 (1968); J. Phys. **A1**, 1563 (1968); J. F. Fernandez and H. A. Gersch, Phys. Rev. **172**, 341 (1968).

¹⁷ R. A. Tahir-Kheli and D. G. McFadden, Phys. Rev. **178**, 800 (1969); **182**, 604 (1969); D. G. McFadden and R. A. Tahir-Kheli, *ibid.* (to be published); and Ref. 10.

¹⁸ See, for example, V. F. Sears [Can. J. Phys. **45**, 2923 (1967)], who showed that for terbium the second moment of the frequency-wave-vector-dependent susceptibility is in considerably better agreement with the observed results at 660°K [data obtained by J. W. Cable, M. F. Collins, and A. D. B. Woods, in Proceedings of the Sixth Rare Earth Reserve Conference, Gatlinburg, Tennessee, 1967 (unpublished)] if the effects of the SRO are taken into account in the form of an additional $(1/T)$ term in the corresponding high temperature series expansion.

* Supported by the U. S. Office of Naval Research.

† Supported by a National Science Foundation predoctoral fellowship.

‡ This work will form part of a dissertation to be submitted to Temple University in partial fulfillment of the requirements of the Ph.D. degree.

¹ L. Van Hove, Phys. Rev. **93**, 268 (1954); **95**, 249 (1954); **95**, 1374 (1954).

² O. Halpern and M. H. Johnson, Phys. Rev. **55**, 898 (1939).

³ G. S. Zhadnov and R. P. Ozerov, Usp. Fiz. Nauk **76**, 239 (1962) [English transl.: Soviet Phys.—Usp. **5**, 104 (1962)].

⁴ Yu. A. Izyumov, Usp. Fiz. Nauk **80**, 41 (1963) [English transl.: Soviet Phys.—Usp. **16**, 359 (1963)].

⁵ F. J. Dyson, Phys. Rev. **102**, 1217 (1956); **102**, 1230 (1956).

⁶ R. A. Tahir-Kheli and D. ter Haar, Phys. Rev. **127**, 95 (1962).

⁷ M. Wortis, Phys. Rev. **138**, A1126 (1965); R. A. Tahir-Kheli, Phys. Letters **12**, 275 (1964).

⁸ H. A. Brown and J. M. Luttinger, Phys. Rev. **100**, 685 (1955); G. S. Rushbrooke and P. J. Wood, Mol. Phys. **1**, 257 (1958); C. Domb and M. F. Sykes, Phys. Rev. **128**, 168 (1962).

In the present paper we attempt to study the SRO effects upon the dynamics of paramagnets. We assume that these paramagnets are well described by a Heisenberg localized spin Hamiltonian. Our work is subject to several distinct types of approximations. First, we construct the dynamical line shapes by using a phenomenological approximation which relies only upon the knowledge of a few low-order frequency moments.¹⁹ The relevance of this phenomenological procedure for studying the long-wavelength small-frequency dynamics of Heisenberg paramagnets was suggested by Bennett and Martin²⁰ and has proved useful in the discussion of the structure of the results even in the neighborhood of the critical point.²¹ Moreover, in the extreme paramagnetic regime, the adequacy of this representation for studying the behavior of the frequency wave-vector-dependent susceptibilities for all wave vectors and frequencies has now been fully discussed for the case of elevated temperatures.¹⁷ For the present it suffices to say that on the whole this procedure seems to give reasonable results for intermediate and high frequencies (i.e., for short and intermediate times), while for small frequencies (i.e., long times), the results are likely to be only qualitatively correct.²²

The second type of approximation to be used in the present work pertains to the determination of the frequency moments themselves. In the literature^{14,15,17} the relevant frequency moments have been computed in the limit that the system temperature $T \rightarrow \infty$. Of course, when the system temperature is at least several times T_c , or higher, it may be an adequate approximation to ignore the remaining terms in the relevant series expansion in powers of T_c/T . The experiments of interest are, however, often carried out at temperatures such that the ratio T_c/T is of the order of $\frac{3}{4}$ to $\frac{1}{4}$. Under these circumstances, it is necessary to compute the first few terms in the series expansion in powers of T_c/T , if the moments are to be determined to adequate accuracy. In the present work, we have computed the zeroth frequency moment $\langle \omega^0 \rangle_{\mathbf{k}}$ exactly to the order $(T_c/T)^4$, the second frequency moment $\langle \omega^2 \rangle_{\mathbf{k}}$ to the order $(T_c/T)^3$, and the fourth frequency moment $\langle \omega^4 \rangle_{\mathbf{k}}$ to the order $(T_c/T)^2$.

In addition to the above two approximations, we have also assumed the lattice to be rigid. This approximation would, of course, have no important effects upon the results if the spin degrees of freedom were

completely independent of the lattice degrees of freedom because then from the experimental slow neutron-scattering data one could (in principle) separate the contributions arising from the lattice vibrations alone. (Note also that in this idealized limit the phonon scattering would arise only due to neutron-nucleus interactions.) In practice, the thermal motion of the atoms in the lattice is implicitly dependent upon the fluctuation of the spin on the atoms and consequently the magnetic scattering of neutrons also contains contributions from the lattice vibrations. Such a magnetovibrational scattering may sometimes be comparable to the strictly magnetic scattering²³ and therefore its contribution to the line shape could then be important. In the paramagnetic regime, however, the hope is that the major contribution from magnetovibrational effects will be nearly elastic²⁴ and will therefore affect the structure of the line shape only in the vicinity of the zero frequency.

Using the techniques discussed in Ref. 17 we have constructed a theoretical line shape for a paramagnet at a few times its critical temperature. These theoretical results are compared with the neutron-scattering experimental results of Windsor, Briggs, and Kestigian²⁰ on RbMnF_3 at about $3.5T_N$. The agreement of the resultant *parameter-free* theoretical results with the corresponding experimental data is generally fair, except at small energy transfers (i.e., at small frequencies) where the consequences of our assumption regarding the absence of magnetovibrational interactions is likely to be the most serious. Moreover, there is also the possibility that some of the discrepancy between the theoretical and the experimental results may in part be due to one of the following causes: First, the crudeness of our phenomenological approximation for the line shape is likely to be especially pronounced in the vicinity of $\omega \rightarrow 0$ where the long-time behavior of the system makes important contributions to the line shape. (Note that guessing precisely the form of the long time behavior of correlation functions from the knowledge of a few low-order frequency moments, i.e., from the known behavior of the correlation functions for very short times, may indeed be expected to be somewhat unreliable.) Secondly, the rather short high-temperature series used here may quite possibly not embody all the relevant SRO effects.

The organization of the paper is as follows. In Sec. II we record some preliminary considerations regarding the theory of inelastic magnetic neutron scattering and its application to paramagnetic Heisenberg-spin systems such as RbMnF_3 . We also introduce the concept of frequency moments and indicate how the presence of SRO causes the shape of $\mathcal{S}(\mathbf{K}, \omega)$ to be asymmetric in ω .

The frequency moments are computed in Sec. III. The influence of the SRO on these moments is examined

¹⁹ That this is somewhat of a dangerous business is clear from the fact that the knowledge of any finite number of frequency moments by themselves does not enable one to construct a unique lineshape for any finite frequency interval. [See for example, W. C. Grant, *Physica* **30**, 1433 (1964).] However, the knowledge of several lowest-order frequency moments can be of great deal of assistance in fixing the parameters that appear in any phenomenological theory of lineshapes where the actual functional form of the lineshape has been derived from intuitive, physical arguments.

²⁰ H. S. Bennett and P. C. Martin, *Phys. Rev.* **138**, A608 (1965).

²¹ H. S. Bennett, *Phys. Rev.* **174**, 629 (1968); **176**, 650 (1968); R. A. Tahir-Kheli, *J. Appl. Phys.* **40**, 1550 (1969).

²² An instructive demonstration of such a likelihood has just been given in a somewhat different context by D. L. Huber, J. S. Semura, and C. G. Windsor, *Phys. Rev.* (to be published).

²³ R. J. Elliott and R. D. Lowde, *Proc. Roy. Soc. (London)* **A230**, 46 (1955).

²⁴ R. D. Lowde, *Proc. Roy. Soc. (London)* **A235**, 305 (1956).

in detail for the particular case of a simple cubic, nearest neighbor Heisenberg paramagnet (with anti-ferromagnetic ground-state ordering) at $T=3.5T_N$. This case corresponds closely to that of RbMnF_3 under conditions of the experiment reported by Windsor, Briggs, and Kestigian.²⁵ Some general remarks about the influence of the SRO on the line shape are made through the examination of these moments.

Using the phenomenological approximation described in our previous work,¹⁷ the line shape is constructed in Sec. IV. The results are again specialized to the case of RbMnF_3 under the aforementioned conditions. The theoretical results are then compared with the corresponding experimental results of Ref. 25.

The concluding Sec. V contains a discussion of the results derived in the preceding sections.

II. PRELIMINARY CONSIDERATIONS

When slow neutrons are scattered from many-body scatterers, they typically undergo energy and momentum transfers of the same order of magnitude as the energies and momenta of the elementary excitations in these systems. For such scattering the first Born approximation holds very well²⁶ and the spectrum of the scattered neutrons is then described by a two-body space-time-dependent statistical correlation function of the scatterer.¹ For the paramagnetic system under discussion here, if we assume that the spin and the lattice degrees of freedom are uncoupled,²³ then the differential magnetic scattering cross section, per unit energy interval and solid angle of the outgoing neutrons, has the following form¹ for unpolarized incident neutrons:

$$\frac{d^2\sigma}{d\Omega'dE'} = N\rho(\mathbf{k},\mathbf{k}') \sum_{\alpha,\alpha'} (\delta_{\alpha,\alpha'} - \hat{K}_\alpha \hat{K}'_{\alpha'}) S^{\alpha\alpha'}(\mathbf{K},\omega), \quad (2.1)$$

$$\alpha, \alpha' \equiv x, y, z,$$

where \mathbf{k} and \mathbf{k}' are wave vectors of the incident and the scattered neutrons, respectively, E and E' are their corresponding kinetic energies, and \mathbf{K} and ω are the momentum and the energy loss suffered by the scattered neutrons, i.e.,

$$\begin{aligned} \mathbf{K} &= \mathbf{k} - \mathbf{k}', \\ \omega &= E - E' \end{aligned} \quad (2.2)$$

(throughout we use Dirac's units where $\hbar=1$). The function $\rho(\mathbf{k},\mathbf{k}')$ is simply related to the total free-spin scattering cross section Na (a is equal to about 0.292 b), and the neutron scattering form factor $f(\mathbf{K})$ of the scattering atoms in the following way:

$$\rho(\mathbf{k},\mathbf{k}') = Na(k'/k) |f(\mathbf{K})|^2. \quad (2.3)$$

The function $S^{\alpha\alpha'}(\mathbf{K},\omega)$ is the momentum-frequency Fourier transform of the spin-correlation function of the

scattering system:

$$S^{\alpha\alpha'}(\mathbf{K},\omega) = \frac{1}{2\pi} \sum_{\mathbf{R}} e^{i\mathbf{K}\cdot\mathbf{R}} \int_{-\infty}^{+\infty} dt e^{-i\omega t} \langle S_0^\alpha(0) S_{\mathbf{R}}^{\alpha'}(t) \rangle. \quad (2.4)$$

The angular brackets in the right-hand side of Eq. (2.4) denote a canonical average over the density matrix of only the spin degrees of freedom of the scatterer,²⁷ i.e.,

$$\langle \dots \rangle = \text{Tr}[e^{-\beta\mathcal{H}} \dots] / \text{Tr} e^{-\beta\mathcal{H}}. \quad (2.5)$$

We assume the Hamiltonian \mathcal{H} to be of the isotropic Heisenberg form, i.e.,

$$\mathcal{H} = - \sum_{f_1, f_2} I(f_1 f_2) \mathbf{S}_{f_1} \cdot \mathbf{S}_{f_2}. \quad (2.6)$$

While much of the following analysis will be quite general and will apply to the case of arbitrary spin magnitudes, arbitrary lattice dimensionality and arbitrary range of the exchange interactions, $I(f_1 f_2)$, in order to particularize the discussion to the case of RbMnF_3 we later assume a three-dimensional simple cubic lattice with $S=5/2$, restrict the range of $I(f_1 f_2)$ to only nearest-neighbor distance when it will be assumed to have the magnitude $I = -0.28 \text{ meV}$.^{25,28}

Under the isotropic Hamiltonian (2.6) correlation $S^{\alpha\alpha'}(\mathbf{K},\omega)$ is diagonal in the indices α and α' . Moreover, in the paramagnetic state, these diagonal correlations are the same for all α 's and as such it suffices to consider only one of the correlations, e.g., $S^{zz}(\mathbf{K},\omega)$.

Using the fluctuation-dissipation theorem,²³ it is convenient to relate the function $S^{zz}(\mathbf{K},\omega)$ to the spectral function $F(\mathbf{K},\omega)$, i.e.,

$$S^{zz}(\mathbf{K},\omega) = F(\mathbf{K},\omega) / (1 - e^{-\beta\omega}), \quad (2.7a)$$

where

$$\begin{aligned} F(\mathbf{K},\omega) &= F(-\mathbf{K},\omega) = -F(\pm\mathbf{K},-\omega) \\ &= \frac{1}{2\pi} \sum_{\mathbf{R}} e^{i\mathbf{K}\cdot\mathbf{R}} \int_{-\infty}^{+\infty} dt e^{i\omega t} \\ &\quad \times \langle [S_0^z(0), S_{\mathbf{R}}^z(t)] \rangle \end{aligned} \quad (2.7b)$$

Because of the evenness of the function $F(\mathbf{K},\omega)/\omega$ in ω , all of its odd frequency moments will trivially vanish. Its even-frequency moments $\langle \omega^{2n} \rangle_{\mathbf{K}}$, i.e.,

$$\langle \omega^{2n} \rangle_{\mathbf{K}} = \int_{-\infty}^{+\infty} \left[\frac{F(\mathbf{K},\omega)}{\omega} \right] \omega^{2n} d\omega, \quad (2.8)$$

can in the usual fashion be computed in terms of time-independent statistical correlation functions for which a well-defined high-temperature expansion scheme exists.^{15,17} These moments are given in Sec. III. For the present, it is only necessary to record the relationship of the moments $\langle \omega^{2n} \rangle_{\mathbf{K}}$ to the frequency moments of the actual line shape $S(\mathbf{K},\omega)$. This is achieved by a straightforward expansion of the de-

²⁵ C. G. Windsor, G. A. Briggs, and M. Kestigian, Proc. Phys. Soc. (London) **1**, 940 (1968).

²⁶ Unless repeated scattering processes become likely as for example happens in nuclear reactor piles.

²⁷ This assumes the absence of all magnetovibrational contributions to the scattering.

²⁸ C. G. Windsor and R. W. H. Stevenson, Proc. Phys. Soc. (London) **87**, 501 (1966); C. G. Windsor, *ibid.* **89**, 825 (1966).

nominator of Eq. (2.7a) in powers of $\beta\omega$, i.e.,

$$\omega_{\mathbf{K}}^{(2n)} = 3\langle\omega^{2n}\rangle_{\mathbf{K}} + \frac{1}{4}\beta^2\langle\omega^{2n+2}\rangle_{\mathbf{K}} - \frac{\beta^4}{240}\langle\omega^{2n+4}\rangle_{\mathbf{K}} \\ + \frac{\beta^6}{10080}\langle\omega^{2n+6}\rangle_{\mathbf{K}} + \dots, \quad (2.9a)$$

$$\omega_{\mathbf{K}}^{(2n+1)} = -\frac{3}{2}\beta\langle\omega^{2n+2}\rangle_{\mathbf{K}} + \dots, \quad (2.9b)$$

where we have used the following notation for the moments of the line shape $\mathcal{S}(\mathbf{K},\omega)$:

$$\int_{-\infty}^{+\infty} \mathcal{S}(\mathbf{K},\omega)\omega^n d\omega \equiv k_B T \omega_{\mathbf{K}}^{(n)}. \quad (2.9c)$$

Clearly, in the limit of infinite temperatures $\beta\mathcal{S}^{zz}(\mathbf{K},\omega)$ and $F(\mathbf{K},\omega)/\omega$ coincide and the line shape $\mathcal{S}^{zz}(\mathbf{K},\omega)$ is symmetric in ω . However, at finite temperatures, the additional terms proportional to higher powers of β have also to be retained. When this is done, even moments of $\beta\mathcal{S}^{zz}(\mathbf{K},\omega)$ turn out to be the same as those of $F(\mathbf{K},\omega)$ to the first two dominant powers of β . [See Eq. (2.9a).] For noninfinite temperatures, i.e., where

SRO effects are taken into account, the function $\mathcal{S}^{zz}(\mathbf{K},\omega)$ is no longer even in ω and therefore also has finite odd moments. These moments are in general smaller than the even moments by a factor β and are proportional to the next higher-order (even) moments of $F(\mathbf{K},\omega)/\omega$ [see Eq. (2.9b)].

III. FREQUENCY MOMENTS

We have calculated the frequency moments, $\langle\omega^{2n}\rangle_{\mathbf{K}}$, $n=0, 1, 2$, under the Hamiltonian (2.6). The procedure for the computation of these moments is in essence similar to that used for the calculation of the infinite temperature results.²⁹ The essential difference is that for finite temperatures the density matrix, ρ ,

$$\rho = e^{-\beta\mathcal{H}}/\text{Tr}e^{-\beta\mathcal{H}}, \quad (3.1)$$

has to be duly computed to the desired accuracy in the power expansion of β , whereas for infinite temperatures it could be replaced by the first term $-\beta\mathcal{H}/\text{Tr}[1]$.

The details of computation are understandably exceedingly tedious. For brevity therefore we only record the final results here: We get

$$\langle\omega^0\rangle_{\mathbf{K}} = \beta X + \beta^2 2X^2 \sum_{\mathbf{R}} e^{i\mathbf{K}\cdot\mathbf{R}} I(\mathbf{R}) + \beta^3 [4X^3 \sum_{\mathbf{R},\mathbf{A}} e^{i\mathbf{K}\cdot\mathbf{R}} I(\mathbf{A}) I(\mathbf{R}-\mathbf{A}) - \frac{1}{3}X^2 \sum_{\mathbf{R}} (e^{i\mathbf{K}\cdot\mathbf{R}} + 14)] \\ + \beta^4 \left\{ 8X^4 \sum_{\mathbf{R},\mathbf{A},\mathbf{B}} e^{i\mathbf{K}\cdot\mathbf{R}} I(\mathbf{A}) I(\mathbf{B}) I(\mathbf{R}+\mathbf{A}+\mathbf{B}) - 16X^4 \sum_{\mathbf{R},\mathbf{A}} e^{i\mathbf{K}\cdot\mathbf{R}} I(\mathbf{R}) I^2(\mathbf{A}) \right. \\ \left. \sum_{\mathbf{R},\mathbf{A}} I(\mathbf{R}) I(\mathbf{A}) I(\mathbf{R}-\mathbf{A}) (-\frac{4}{3}X^3 - 8X^4) + 4X^3 \sum_{\mathbf{R},\mathbf{A}} e^{i\mathbf{K}\cdot\mathbf{R}} I^2(\mathbf{A}) (I(\mathbf{R}-\mathbf{A}) - I(\mathbf{R})) \right. \\ \left. + \sum_{\mathbf{R}} \left[\left(\frac{16}{5}X^4 + \frac{8}{5}X^3 + \frac{2}{5}X^2 \right) e^{i\mathbf{K}\cdot\mathbf{R}} + \frac{2}{5}X^3 - \frac{4}{15}X^2 \right] I^3(\mathbf{R}) \right\} + o(\beta^5), \quad (3.2)$$

$$\langle\omega^2\rangle_{\mathbf{K}} = 8\beta X^2 \sum_{\mathbf{R}} (1 - e^{i\mathbf{K}\cdot\mathbf{R}}) I^2(\mathbf{R}) + 16\beta^2 X^3 \sum_{\mathbf{R},\mathbf{A}} (1 - e^{i\mathbf{K}\cdot\mathbf{R}}) I(\mathbf{R}) I(\mathbf{A}) I(\mathbf{R}-\mathbf{A}) - 4\beta^2 X^2 \sum_{\mathbf{R}} (1 - e^{i\mathbf{K}\cdot\mathbf{R}}) I^3(\mathbf{R}) \\ + \frac{2}{3}\beta^3 \left[\sum_{\mathbf{R}} (1 - e^{i\mathbf{K}\cdot\mathbf{R}}) I^4(\mathbf{R}) \left(\frac{96}{5}X^4 + \frac{4}{5}X^2 \right) - 96X^4 \sum_{\mathbf{R}} (1 - e^{i\mathbf{K}\cdot\mathbf{R}}) I^2(\mathbf{R}) \sum_{\mathbf{A}} I^2(\mathbf{A}) \right. \\ \left. - 8X^3 \sum_{\mathbf{R},\mathbf{A}} (1 - e^{i\mathbf{K}\cdot\mathbf{R}}) I^2(\mathbf{R}) I(\mathbf{A}) I(\mathbf{R}-\mathbf{A}) + 48X^4 \sum_{\mathbf{R},\mathbf{A},\mathbf{B}} (1 - e^{i\mathbf{K}\cdot\mathbf{R}}) I(\mathbf{R}) I(\mathbf{A}) I(\mathbf{B}) I(\mathbf{R}+\mathbf{A}+\mathbf{B}) \right] + o(\beta^4), \quad (3.3)$$

$$\frac{\langle\omega^4\rangle_{\mathbf{K}}}{32\beta X^3} = \sum_{\mathbf{R}} (e^{i\mathbf{K}\cdot\mathbf{R}} - 1) I^4(\mathbf{R}) (4 + 1/2X) + \sum_{\mathbf{R},\mathbf{A}} \{ I^2(\mathbf{R}) (1 - e^{i\mathbf{K}\cdot\mathbf{R}}) I^2(\mathbf{A}) (7 - 3e^{i\mathbf{K}\cdot\mathbf{A}}) \\ + 2I(\mathbf{R}) I(\mathbf{A}) I(\mathbf{R}-\mathbf{A}) [2e^{i\mathbf{K}\cdot\mathbf{R}} I(\mathbf{R}-\mathbf{A}) - e^{i\mathbf{K}\cdot\mathbf{R}} I(\mathbf{R}) - I(\mathbf{R})] \} \\ + \frac{16}{5}\beta X \sum_{\mathbf{R}} (1 - e^{i\mathbf{K}\cdot\mathbf{R}}) I^5(\mathbf{R}) + 2\beta X \sum_{\mathbf{R},\mathbf{A}} \left[2I(\mathbf{R}) I(\mathbf{A})^2 I(\mathbf{R}-\mathbf{A}) (e^{i\mathbf{K}\cdot(\mathbf{R}-\mathbf{A})} + 1 - 2e^{i\mathbf{K}\cdot\mathbf{R}}) \right. \\ \left. + 4I^3(\mathbf{R}) I^2(\mathbf{A}) (e^{i\mathbf{K}\cdot\mathbf{R}} - 1 - e^{i\mathbf{K}\cdot(\mathbf{R}-\mathbf{A})} + e^{i\mathbf{K}\cdot\mathbf{A}}) + \frac{84}{5} (e^{i\mathbf{K}\cdot\mathbf{R}} - 1) I^3(\mathbf{R}) I(\mathbf{A}) I(\mathbf{R}-\mathbf{A}) \right] \\ + 2\beta X \sum_{\mathbf{R},\mathbf{A},\mathbf{B}} [I(\mathbf{A}) I(\mathbf{R}) I(\mathbf{B}) I(\mathbf{R}+\mathbf{A}) I(\mathbf{R}+\mathbf{B}) (-3e^{i\mathbf{K}\cdot\mathbf{R}} + 6e^{i\mathbf{K}\cdot(\mathbf{R}+\mathbf{A})} - 2 - e^{i\mathbf{K}\cdot(\mathbf{R}+\mathbf{A}+\mathbf{B})}) \\ + 2I(\mathbf{A}) I(\mathbf{B})^2 I(\mathbf{R}) (2e^{i\mathbf{K}\cdot(\mathbf{R}+\mathbf{B})} - e^{i\mathbf{K}\cdot(\mathbf{R}+\mathbf{A}+\mathbf{B})} - e^{i\mathbf{K}\cdot\mathbf{R}}) \\ + 2I^2(\mathbf{R}) I(\mathbf{A}) I(\mathbf{B}) I(\mathbf{A}+\mathbf{R}+\mathbf{B}) (-e^{i\mathbf{K}\cdot\mathbf{R}} + 3e^{i\mathbf{K}\cdot(\mathbf{R}+\mathbf{A})} - 2e^{i\mathbf{K}\cdot\mathbf{B}}) \\ + 2I^2(\mathbf{R}) I(\mathbf{A}) I(\mathbf{B}) I(\mathbf{A}-\mathbf{B}) (6 - 5e^{i\mathbf{K}\cdot\mathbf{R}} - 5e^{i\mathbf{K}\cdot\mathbf{B}} + 3e^{i\mathbf{K}\cdot(\mathbf{A}+\mathbf{R})} + e^{i\mathbf{K}\cdot(\mathbf{A}+\mathbf{B})})]$$

²⁹ See for example Refs. 14 and 17.

$$\begin{aligned}
& +\beta\frac{136}{5}\sum_{\mathbf{R}}(1-e^{i\mathbf{K}\cdot\mathbf{R}})I^5(\mathbf{R})+\frac{\beta}{2}\sum_{\mathbf{R},\mathbf{A}}[(1-e^{i\mathbf{K}\cdot(\mathbf{R}+\mathbf{A})})(I(\mathbf{R})I(\mathbf{A}))^2I(\mathbf{R}+\mathbf{A}) \\
& +I^3(\mathbf{R})I(\mathbf{A})I(\mathbf{R}+\mathbf{A})(7e^{i\mathbf{K}\cdot\mathbf{R}}-4e^{i\mathbf{K}\cdot\mathbf{A}}-3)+I^3(\mathbf{R})I^2(\mathbf{A})(10e^{i\mathbf{K}\cdot\mathbf{R}}-14-8e^{i\mathbf{K}\cdot(\mathbf{R}+\mathbf{A})}+12e^{i\mathbf{K}\cdot\mathbf{A}})] \\
& +\frac{7\beta}{40X}\sum_{\mathbf{R}}(1-e^{i\mathbf{K}\cdot\mathbf{R}})I^5(\mathbf{R})+{}_0(\beta^2). \quad (3.4)
\end{aligned}$$

The foregoing results, i.e., Eqs. (3.2)–(3.4), are valid for arbitrary range of the exchange interaction $I(\mathbf{R})$ and for arbitrary lattice structure and dimensionality. While this general form is useful to record, for the problem in hand we need to specialize to the case of a simple cubic lattice with lattice constant a_0 and only nearest-neighbor exchange interaction I . Because the relevant algebra for obtaining this specialization is somewhat tedious to carry out from the results for the general case listed in Eqs. (3.2)–(3.4), we give below the final form of the relevant expressions,

$$\langle\omega^0\rangle_{\mathbf{K}}=\beta X\left[1+\frac{1}{3}\theta C+\theta^2\left(\frac{1}{9}C^2-(C+42)/216X\right)+\theta^3\left[C^3/27-29C/270+(4C^2-56C/5+\frac{3}{5})/432X\right.\right. \\
\left.\left.+\left(\frac{1}{5}C-\frac{2}{5}\right)/432X^2\right]+{}_0(\theta^4)\right], \quad (3.5)$$

$$\langle\omega^2\rangle_{\mathbf{K}}=16\beta I^2 X^2(3-C)\left[1-\frac{\theta}{24X}+\frac{\theta^2}{2160}(204+1/X^2)+{}_0(\theta^3)\right], \quad (3.6)$$

$$\begin{aligned}
\frac{\langle\omega^4\rangle_{\mathbf{K}}}{128\beta I^4 X^3} & = (3-C)(19-3C-1/4X)+\frac{1}{6}\theta\left[-4C^3+20C^2-(289/5)C+57/5+6(C_x^2+C_y^2+C_z^2)\right. \\
& \left.+24(C_x C_y+C_x C_z+C_y C_z)\right]+(\theta/12X)(-111/5+(97/5)C-4C^2)+7\theta(3-C)/960X^2+{}_0(\theta^2), \quad (3.7)
\end{aligned}$$

where

$$X=\frac{1}{3}S(S+1), \quad (3.8)$$

$$\theta=12X\beta I, \quad (3.9)$$

$$C_x=\cos(K_x a_0), \quad C_y=\cos(K_y a_0), \quad C_z=\cos(K_z a_0), \quad (3.10)$$

$$C=C_x+C_y+C_z. \quad (3.11)$$

Using Eqs. (2.9a)–(2.9c) we can now find the frequency moments of the spectral line shape $\mathcal{S}(\mathbf{K},\omega)$, i.e., $\omega_{\mathbf{K}}^{(n)}$. When this is done we find that the result for $\omega_{\mathbf{K}}^{(2)}$ is in disagreement with that given by Sears.¹⁸ (Sears's result is also quoted in Refs. 15 and 25. Note that Sears's result can be taken over to find our $\omega_{\mathbf{K}}^{(0)}$ and $\omega_{\mathbf{K}}^{(2)}$ to the first two dominant powers in β and our disagreement with his result arises³⁰ only in the order β^2 for $\omega_{\mathbf{K}}^{(2)}$. Note also that we have computed our results to one additional order in β , i.e., to β^3 , for $\omega_{\mathbf{K}}^{(2)}$ and two additional orders in β , i.e., to β^4 , for $\omega_{\mathbf{K}}^{(0)}$ than the corresponding results of Sears for the isotropic Hamiltonian being used here.)

To get a feel for how the line shape, $\mathcal{S}(\mathbf{K},\omega)$, changes due to the presence of SRO, we have used Eqs. (2.9a)–(2.9c) and (3.5)–(3.7) to convert to the frequency moments $\omega_{\mathbf{K}}^{(n)}$. For the special case of a simple cubic antiferromagnet with only a nearest-neighbor isotropic Heisenberg exchange, $I=-0.28$ meV, $S=\frac{5}{2}$, at a temperature of 293°K, the results for the corresponding moments are given in Tables I and II. To get an estimate of the convergence of the high-temperature series expansion for the relevant moments, we have listed the contributions arising from the various additional β

³⁰ It is interesting to note that if one made the mistake of assuming quantum mechanical traces of the form $\text{Tr}(S_\sigma^z S_\sigma^y S_\sigma^z)$ to be vanishing, one would get the same result as recorded by Sears for the Heisenberg Hamiltonian without single ion anisotropy, i.e., for the Hamiltonian that is being used here.

dependent terms. For convenience, in the case of even-order moments, these additional contributions have been listed as percentages of the infinite-temperature moments. Because the odd-order moments are vanishing in the limit of infinite temperature and because their temperature corrections are determined in terms of the even-order moments, we have not listed them separately. The various \mathbf{K} values used in these tables were chosen to correspond to the actual cases studied experimentally by Windsor *et al.*²⁵

A perusal of Tables I and II readily leads to the following conclusions: For small \mathbf{K} values (henceforth \mathbf{K} denotes only the reduced wave vector)³¹ the first SRO correction to the zeroth moment, $\omega_{\mathbf{K}}^{(0)}$, is always negative and is typically of the order of 30%. The second SRO correction to $\omega_{\mathbf{K}}^{(0)}$ is positive and is typically $\frac{1}{3}$ rd to $\frac{1}{4}$ th of the first-order correction. The third-order correction to $\omega_{\mathbf{K}}^{(0)}$ is again negative and is typically about $\frac{1}{10}$ th to $1/15$ th the first-order correction. The high-temperature series for $\omega_{\mathbf{K}}^{(0)}$ is therefore adequately convergent and therefore for small \mathbf{K} we may expect the over-all effect of SRO to be a reduction of the area under $\mathcal{S}(\mathbf{K},\omega)$ of about 20%.

The first SRO correction to the second moment is always slightly positive, being about 0.55%, for all \mathbf{K} values. (Note that because this correction is so small,

³¹ Because of the fact that $\mathcal{S}(\mathbf{K},\omega)$ is the inverse lattice Fourier transform of the spin correlation function relating to a simple cubic lattice, therefore it has the periodicity of the reciprocal lattice which is also simple cubic in structure. It is convenient to replace the wave vector \mathbf{K} by the reduced vector equal to $\mathbf{K}-\boldsymbol{\tau}$, where $\boldsymbol{\tau}$ is the corresponding vector to the center of any of the nearest reciprocal-lattice zones. Note that in contrast to the full paramagnetic lattice, the antiferromagnetic real lattice has the symmetry of an fcc lattice and as such the relevant inverse lattice has body-centered-cubic symmetry. No confusion should be caused by our using the same symbol, \mathbf{K} , for both the wave vector and the reduced wave vector.

the accuracy of the Marshall-Lowde¹⁵ statement, which was based on Sears's erroneous observation that the first SRO to $\omega_{\mathbf{K}}^{(2)}$ for a nearest-neighbor isotropic Heisenberg paramagnet is zero at all temperatures, is not materially affected.) The second SRO correction to $\omega_{\mathbf{K}}^{(2)}$ is only slightly \mathbf{K} dependent and is generally of the order of about 2% of the infinite-temperature value. The convergence of our high-temperature series is therefore somewhat unimpressive for $\omega_{\mathbf{K}}^{(2)}$ but on intuitive grounds we do believe that the higher-order corrections (if computed) would not alter the result of the first two corrections too drastically. In any event, it is reasonable to assume that the SRO changes the second frequency moment by only a modest amount, i.e., at the temperature of interest, $T=3.5T_N$, the SRO modifications will be a few percent only.

For the fourth-frequency moment $\omega_{\mathbf{K}}^{(4)}$, we have computed only the first-order SRO correction; the computation of additional corrections being exceedingly tedious. The correction is relatively moderate, i.e., about 8–9%. Unfortunately, no reliable statements can be made about the size of the additional SRO corrections and we as such only make a somewhat innocuous assumption that the relative change in the fourth moment due to the SRO is somewhat smaller than that for the zeroth moment and somewhat larger than that for the second moment.

In view of the above discussion it is clear that for small values of \mathbf{K} (to which the above remarks relate) the effects of the SRO are largely to deplete the area under $\delta(\mathbf{K},\omega)$ near the center, i.e., for small frequencies. Since the higher-frequency moments are less sensitive to changes of the shape close to the center one might expect that only a small fraction of the depleted area near the center is distributed to regions of somewhat higher frequencies. This crude picture would then

TABLE I. Finite temperature corrections to the frequency moments of $\delta(\mathbf{K},\omega)$ for small \mathbf{K} -vectors (see Fig. 1). These corrections are expressed as percentages of the infinite temperature moments and refer to the case of interest, i.e., a simple cubic Heisenberg paramagnet with nearest-neighbor isotropic exchange ($I=-0.28$ meV, $T=3.5T_N$, $S=\frac{5}{2}$, and lattice constant = 4.240 Å. The notation used is such that Δ_n' represents the first temperature correction to the n th frequency moment of $\delta(\mathbf{K},\omega)$ given as percentage of the infinite temperature result, Δ_n'' the second correction similarly expressed as percentage of the infinite temperature result and so on. Δ_n^T represents the total percent correction to the n th frequency moment of $\delta(\mathbf{K},\omega)$ from the terms calculated. The first correction to the second frequency moment of $\delta(\mathbf{K},\omega)$, i.e., Δ_2' , is always 0.55%. Therefore $\Delta_2^T = \Delta_2'' + 0.55$. Since we have calculated only one correction to the fourth moment, $\Delta_4^T = \Delta_4'$. We have taken the K vector to be along the line $K_x = K_y$ with $K_z = 0$ so that $K_{110} = \sqrt{2}K_x = |\mathbf{K}|_{\text{expt}}$ (the subscript expt denotes experimental).

| | $K_{110}=0.08$ | $K_{110}=0.16$ | $K_{110}=0.26$ | $K_{110}=0.35$ |
|---------------|----------------|----------------|----------------|----------------|
| Δ_0' | -38.08 | -35.88 | -31.39 | -25.86 |
| Δ_0'' | 13.48 | 11.85 | 8.84 | 5.69 |
| Δ_0''' | -3.69 | -2.88 | -1.56 | 0.45 |
| Δ_0^T | -28.29 | -26.91 | -24.11 | -19.72 |
| Δ_2'' | 1.90 | 1.93 | 1.98 | 2.04 |
| Δ_4' | 8.87 | 9.12 | 9.17 | 8.56 |

TABLE II. Same as in Table I except that this table refers to larger \mathbf{K} vectors (see Fig. 2). The experimental data on the scattering is again taken in such a way that \mathbf{K} lies in the 110 plane. However, now the \mathbf{K} -values used in the theory are such that $K_{110} = \sqrt{2}K_x = |\mathbf{K}|_{\text{expt}}$ and $K_z = |K_z|_{\text{expt}}$. The experimental K -components are always within ± 0.1 Å of the listed values.

| K_{110} | $K_z =$ | 0.1 | 0.3 | 0.5 | 0.7 |
|-----------|---------------|--------|--------|--------|--------|
| 0.1 | Δ_0' | -36.50 | -28.52 | -17.96 | -11.97 |
| | Δ_0'' | 12.30 | 7.12 | 2.24 | 0.46 |
| | Δ_0''' | -3.10 | -0.91 | 0.33 | 0.44 |
| | Δ_0^T | -27.30 | -22.31 | -15.39 | -11.07 |
| | Δ_2'' | 1.92 | 2.01 | 2.13 | 2.19 |
| 0.3 | Δ_4' | 8.98 | 9.67 | 8.43 | 6.94 |
| | Δ_0' | -27.89 | -19.91 | -9.35 | -3.36 |
| | Δ_0'' | 6.77 | 2.97 | -0.10 | -0.85 |
| | Δ_0''' | -0.79 | 0.21 | 0.40 | 0.17 |
| | Δ_0^T | -21.91 | -16.73 | -9.05 | -4.04 |
| 0.5 | Δ_2'' | 2.02 | 2.11 | 2.22 | 2.29 |
| | Δ_4' | 8.62 | 6.76 | 3.94 | 1.95 |
| | Δ_0' | -13.70 | -5.72 | 4.84 | 10.82 |
| | Δ_0'' | 0.89 | -0.63 | -0.71 | 0.24 |
| | Δ_0''' | 0.44 | 0.27 | -0.25 | -0.46 |
| 0.7 | Δ_0^T | -12.37 | -6.08 | 3.88 | 10.60 |
| | Δ_2'' | 2.17 | 2.26 | 2.38 | 2.45 |
| | Δ_4' | 5.25 | 1.62 | -2.95 | -5.63 |
| | Δ_0' | 1.15 | 9.13 | 19.69 | 25.68 |
| | Δ_0'' | -0.94 | 0.11 | 2.96 | 5.68 |
| 0.9 | Δ_0''' | -0.06 | -0.41 | 0.32 | 0.27 |
| | Δ_0^T | 0.15 | 8.83 | 22.97 | 31.63 |
| | Δ_2'' | 2.34 | 2.43 | 2.54 | 2.61 |
| | Δ_4' | -0.51 | -4.94 | -10.51 | -13.65 |
| | Δ_0' | 11.51 | 19.49 | 30.05 | 36.04 |
| | Δ_0'' | 0.39 | 2.88 | 8.13 | 12.10 |
| | Δ_0''' | -0.47 | -0.33 | 1.03 | 2.64 |
| | Δ_0^T | 11.43 | 22.04 | 39.21 | 50.78 |
| | Δ_2'' | 2.45 | 2.54 | 2.66 | 2.73 |
| | Δ_4' | -5.32 | -10.06 | -16.05 | -19.40 |

explain a small increase in $\omega_{\mathbf{K}}^{(2)}$ and a somewhat bigger increase in $\omega_{\mathbf{K}}^{(4)}$, which is much more sensitive to the structure of the wings.

It should be mentioned that qualitatively the above ideas are not in any serious contradiction with the guess of Marshall and Lowde¹⁵ who conjectured that the effects of SRO would be to deplete (for the antiferromagnetic case under study) the area at $\omega=0$ for small \mathbf{K} (and to increase it for large \mathbf{K}) values—much as a Dirac δ function with suitable amplitude would—and to uniformly renormalize the line shape for nonzero frequencies. Quantitatively, however, our results differ from this picture in two respects. First, the total depletion (for small \mathbf{K} values) of the area under the curve is clearly about a third smaller than that anticipated in Ref. 15. Secondly, the renormalization of the finite frequency line shape is *not likely to be frequency independent* because due to the SRO the relative change in the fourth frequency moment is clearly quite different than that in the second frequency moment.

IV. LINE SHAPE

Using the phenomenological approximation whereby the generalized, frequency wave-vector-dependent

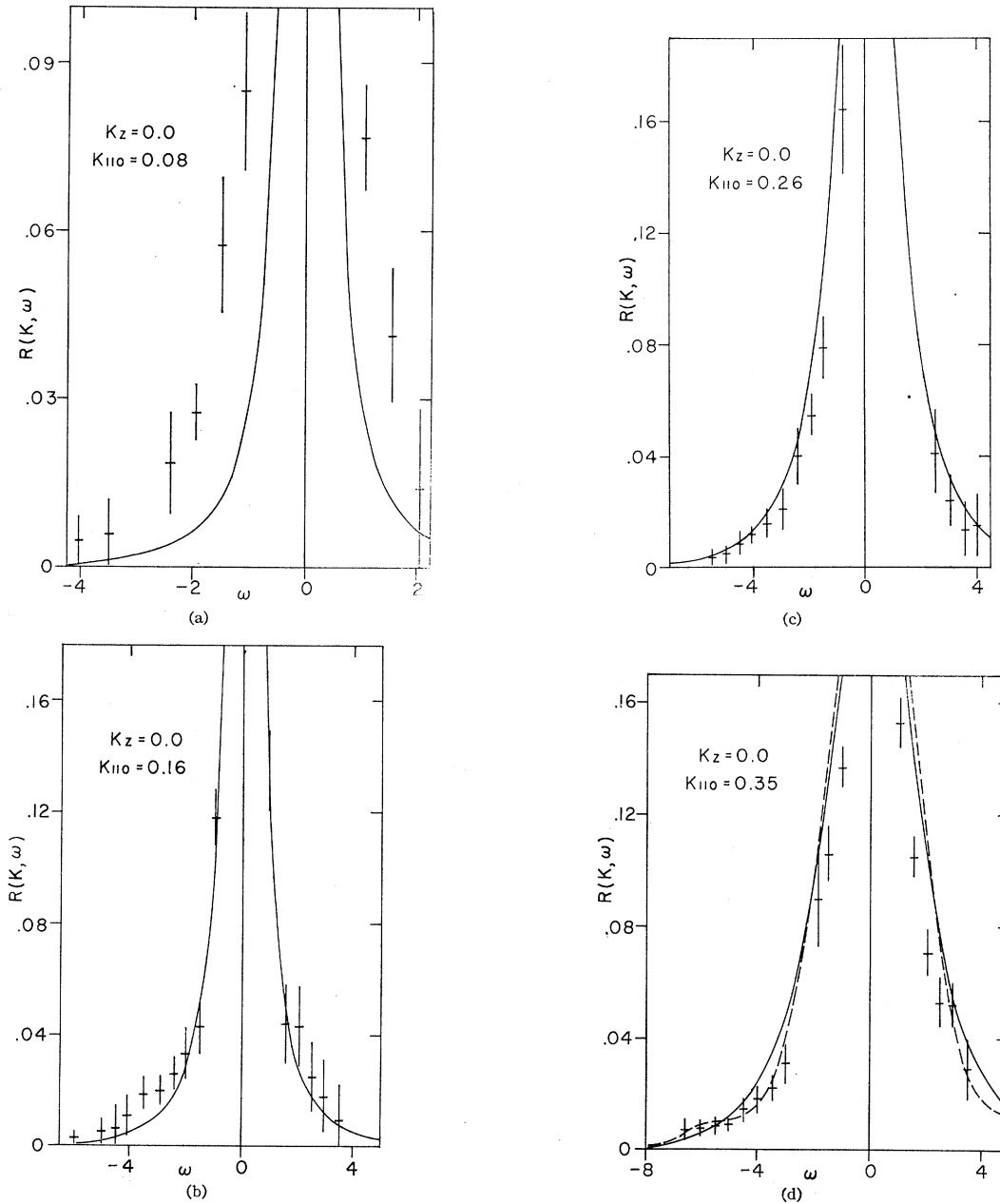


FIG. 1. Plots of the scattering function, $R(\mathbf{K}, \omega) = \mathcal{S}(\mathbf{K}, \omega) / 3X$, in meV^{-1} , versus the frequency, in meV , for small \mathbf{K} vectors. The scattering is in the (110) plane with $K_z = 0$. The \mathbf{K} vectors used in the calculations of the line shape are those listed. The experimental \mathbf{K} values average out to give the listed \mathbf{K} values. The solid curves are based on the two parameter Gaussian approximation for the generalized diffusivity. The dashed curve in Fig. 1(a) is based on the Gram-Charlier series representation of the line shape [this is not shown in Figs. 1(a)–1(c) because it is negative in certain regions and therefore nonphysical].

diffusivity is represented as a two-parameter Gaussian,^{17,20,21,32} we can construct an expression for $F(\mathbf{K}, \omega)$ which conserves the first five frequency moments $\langle \omega^n \rangle_{\mathbf{K}}$, for $n = 0, \dots, 5$. Then using Eq. (2.7a) we can find the line shape $\mathcal{S}^{zz}(\mathbf{K}, \omega)$. The final result is

³² See for example, P. C. Martin, in *1967 Les Houches Lectures: Many Body Problem*, edited by C. De Witt and R. Balian (Gordon and Breach, Science Publishers, Inc., New York, 1968).

$$\mathcal{S}(\mathbf{K}, \omega) = 3\mathcal{S}^{zz}(\mathbf{K}, \omega)$$

$$= 3(1 - e^{-\beta\omega})^{-1} (\omega/\pi) \langle \omega^0 \rangle_{\mathbf{K}} D(\mathbf{K}, \omega) /$$

$$\left[\omega - (2/\sqrt{\pi}) D(\mathbf{K}, \omega) \int_0^{\omega\Gamma(\mathbf{K})} dx e^x \right]^2 + [D(\mathbf{K}, \omega)]^2, \quad (4.1)$$

where

$$D(\mathbf{K}, \omega) = \sqrt{\pi} \Gamma(\mathbf{K}) \langle \omega^2 \rangle_{\mathbf{K}} e^{-\omega^2 \Gamma^2(\mathbf{K})} / \langle \omega^0 \rangle_{\mathbf{K}}, \quad (4.2)$$

and

$$\Gamma(\mathbf{K}) = \left[\frac{\langle \omega^0 \rangle_{\mathbf{K}} \langle \omega^2 \rangle_{\mathbf{K}}}{2[\langle \omega^0 \rangle_{\mathbf{K}} \langle \omega^4 \rangle_{\mathbf{K}} - (\langle \omega^2 \rangle_{\mathbf{K}})^2]} \right]^{1/2}. \quad (4.3)$$

Note that Eqs. (4.2) and (4.3) depend only upon the ratios of the moments $\langle \omega^{2n} \rangle_{\mathbf{K}} / \langle \omega^0 \rangle_{\mathbf{K}}$ for $n=1$ and 2. As the fourth moment is known only to the accuracy

of the first two dominant terms in the high-temperature series expansion, therefore for the sake of consistency we have only the first two terms in the corresponding high-temperature series expansions of the second and the zeroth moments. Within this first-order SRO approximation—whereby the results for the frequency moments themselves are likely to be accurate to about 15% at the temperature of interest, i.e., $T=3.5T_N$ —we have numerically computed the line shape $S(\mathbf{K}, \omega)$ for

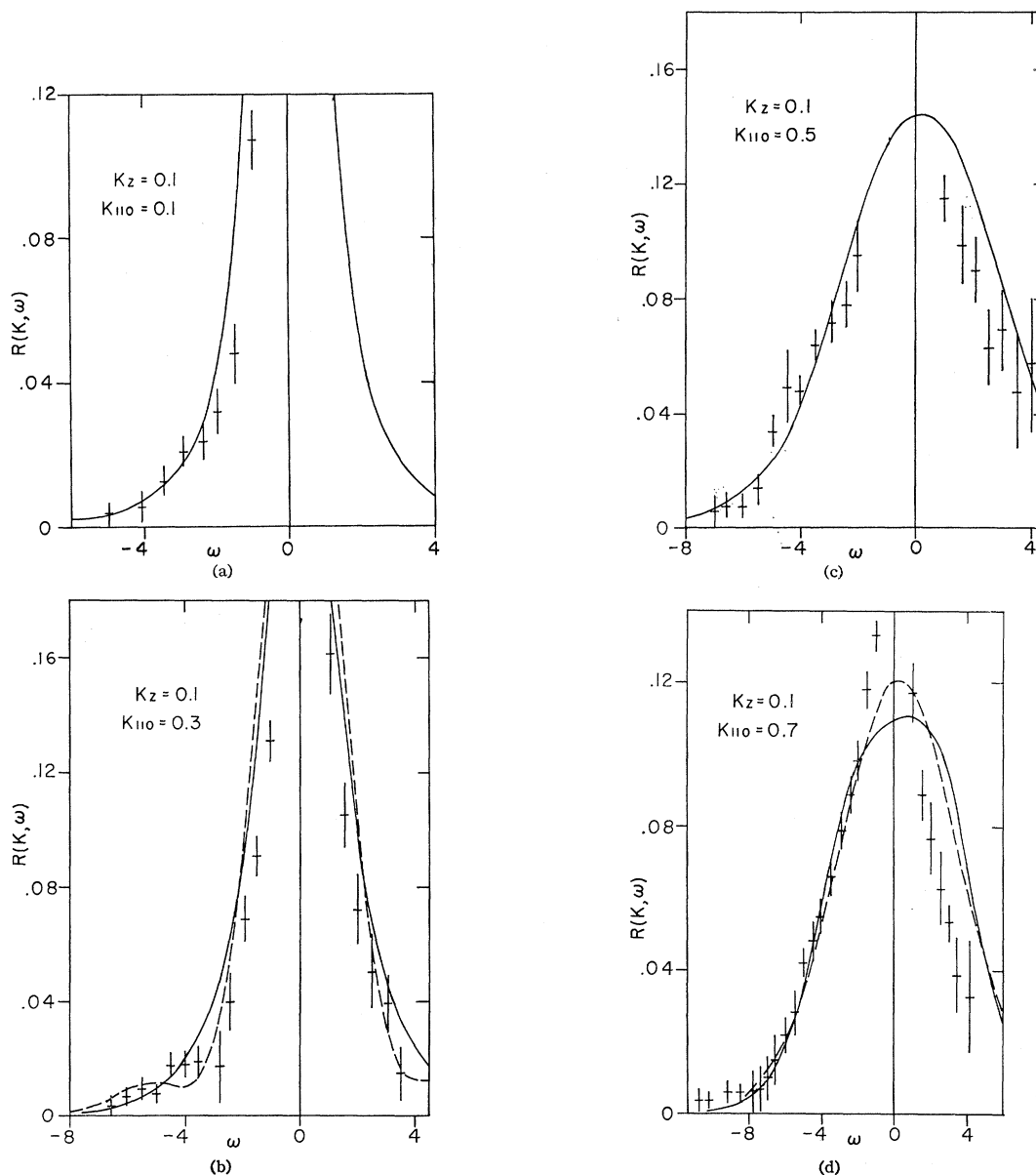


FIG. 2. Plot of $R(\mathbf{K}, \omega) = S(\mathbf{K}, \omega) / 3X$ (in meV^{-1}) versus the frequency (in meV) for various \mathbf{K} vectors as listed. The scattering is within the (110) plane. Consequently, $K_x = K_y = K_{110} / \sqrt{2}$. The experimental values of the components of the \mathbf{K} vectors (i.e., K_{110} and K_z) are centered (to within $\pm 0.1 \text{ \AA}$) around the listed K vectors. The solid curves are the result of the two-parameter approximation for the generalized diffusivity and the dashed curve the result of the Gram-Charlier series. The Gram-Charlier series result does not appear in Fig. 2(a) because it has a negative region for small \mathbf{K} values and so is nonphysical. The two curves are almost identical in Figs. 2(c), 2(g), 2(k), 2(l), and 2(p) and so the line shape based on the Gram-Charlier series is not recorded separately.

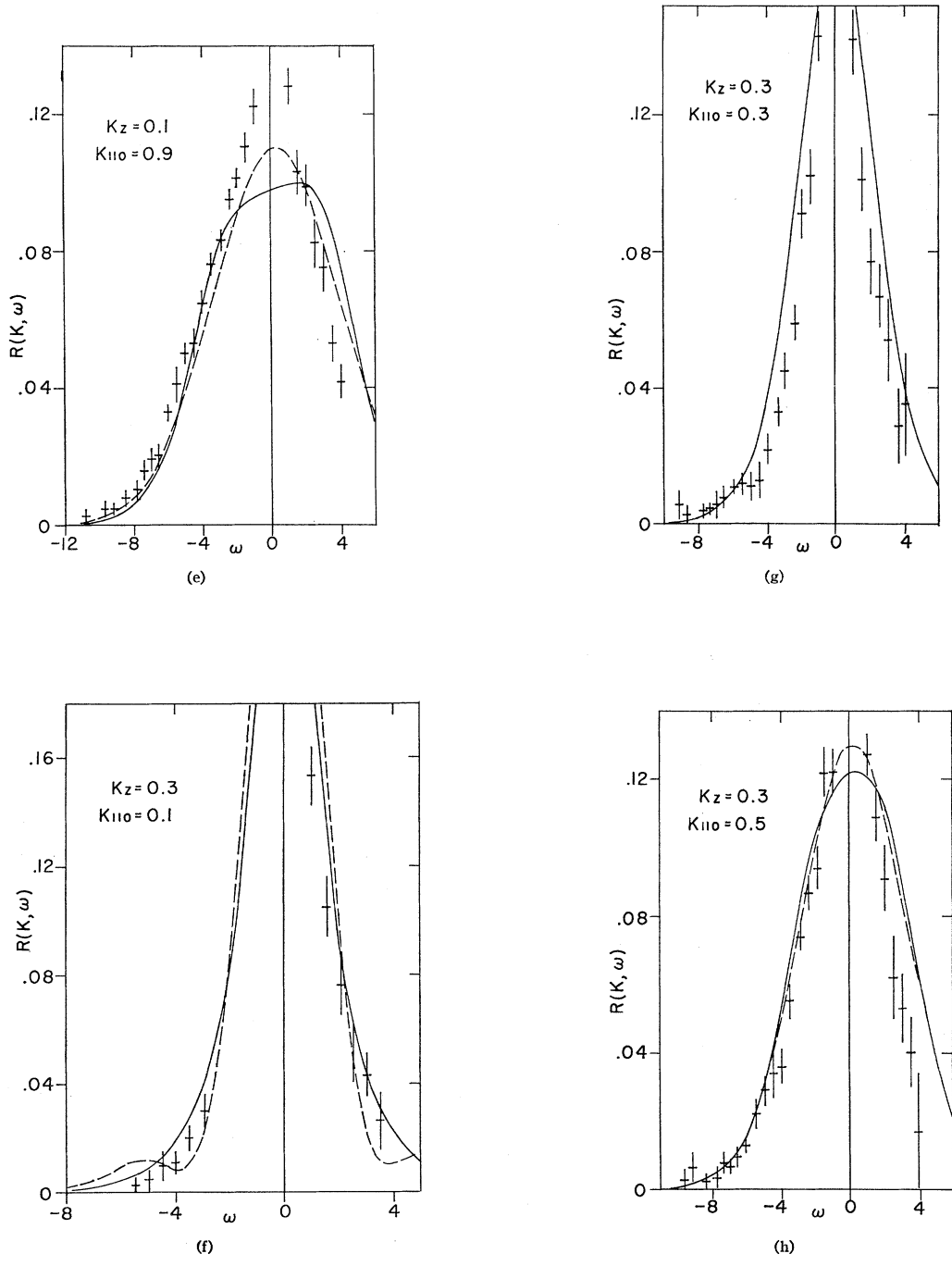


FIG. 2 (continued)

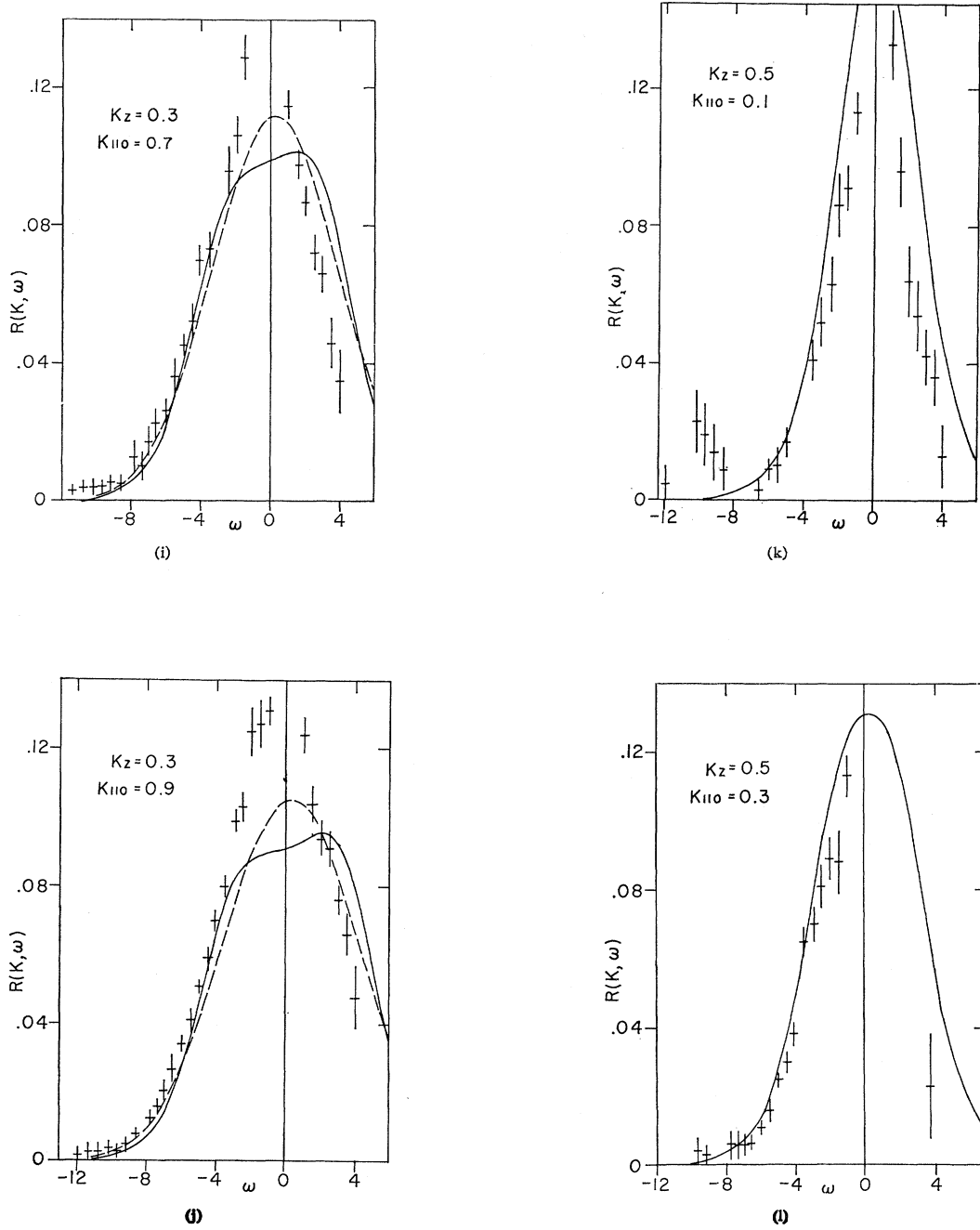


FIG. 2 (continued)

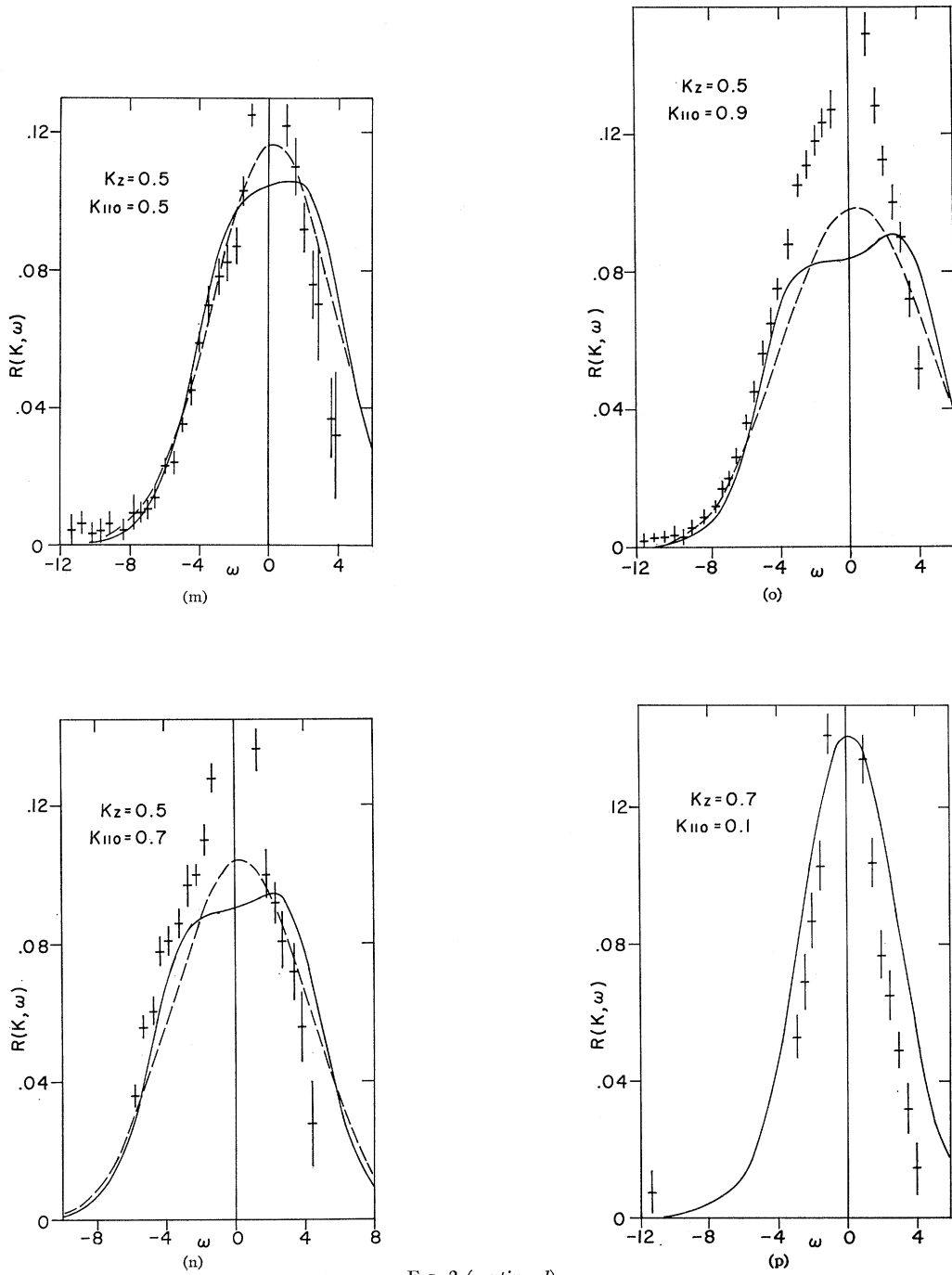


FIG. 2 (continued)

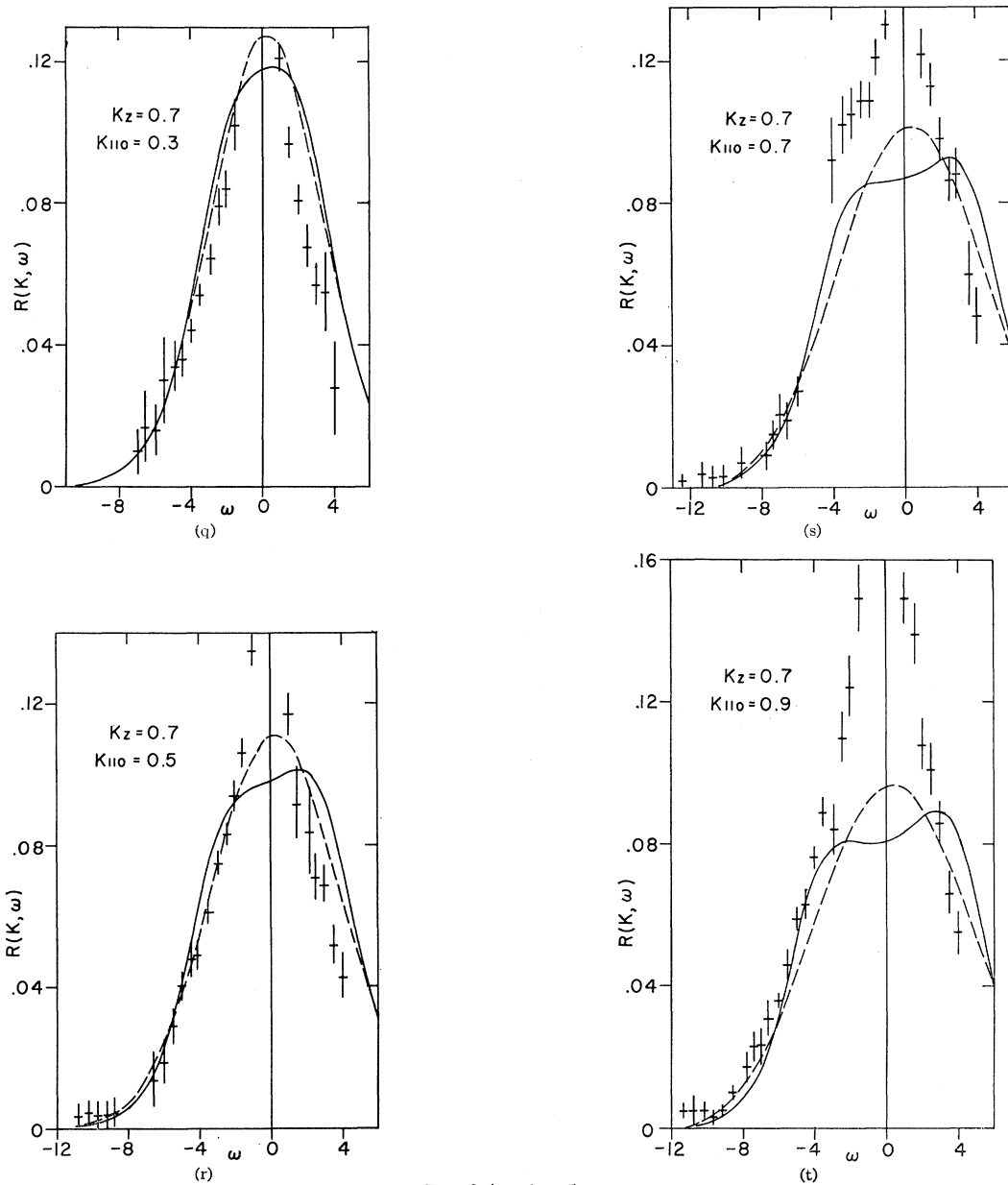


FIG. 2 (continued)

various values of \mathbf{K} which are of interest in analyzing the experimental data of Windsor *et al.*²⁵

It should be emphasized that because the line shape $\mathcal{S}(\mathbf{K}, \omega)$ is renormalized by the factor $\langle \omega^0 \rangle_{\mathbf{K}}$ [see Eq. (4.1) and note that except for this factor in the numerator, the rest of the expression only involves ratios of the moments $\langle \omega^{2n} \rangle_{\mathbf{K}} / \langle \omega^0 \rangle_{\mathbf{K}}$], and because the first two terms in the high-temperature series expansion for $\langle \omega^0 \rangle_{\mathbf{K}}$ in general represent the zeroth moment only to an accuracy of about 10%, the area under our computed curves for $\mathcal{S}(\mathbf{K}, \omega)$ will also be incorrect by about this amount. And this inaccuracy in the area is over and above the possible inaccuracy in the frequency de-

pendent shape of the curve $\mathcal{S}(\mathbf{K}, \omega)$. We have plotted the approximate line shape $\mathcal{S}(\mathbf{K}, \omega)$ in Figs. 1 and 2 and the results are displayed so that they may be readily compared with the experimental determination of the corresponding lineshape from the neutron-scattering experiments of Windsor *et al.* The agreement between the experimental and the parameter-free theoretical results is in general reasonable considering the possible inaccuracy, i.e., up to about 15%, of the frequency moments and the fact that we are using an approximate, phenomenological procedure for constructing the line shape.

It is interesting to compare these two-parameter

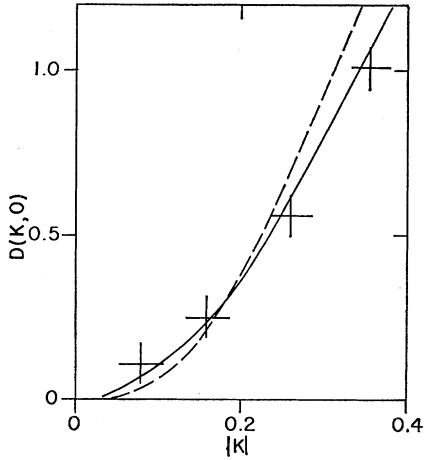


FIG. 3. Plot of $D(\mathbf{K}, \omega=0)$ versus the magnitude of the wave vector \mathbf{K} . The experimental points are obtained from the widths of the best fitting Lorentzian line shapes to the experimental data in Fig. 1. The curves are based on the two parameter Gaussian approximation for the generalized diffusivity. Both curves refer to the case of experimental interest, i.e., $S = \frac{5}{2}$ and $I = -0.28$ meV but the solid curve is for infinite temperature while the dashed curve utilizes the first temperature correction for the frequency moments for RbMnF_3 with $T = 293^\circ\text{K}$. The results are essentially isotropic for these small K vectors (we have used $K_x = K_y, K_z = 0$, so that $|\mathbf{K}| = \sqrt{2}K_x$). The discrepancy between the experimental results and the theoretical (dashed) curve are not too great. Indeed, the differences are within the accuracy expected considering that our theoretical result is subject to the various uncertainties discussed in Sec. V.

Gaussian diffusivity results with the predictions of the Gram-Charlier series representation. This representation was suggested by Collins and Marshall¹⁴ and its extension to finite temperatures should yield the following form:

$$S(\mathbf{K}, \omega) = \frac{3\omega X \langle \omega^0 \rangle_{\mathbf{K}}}{1 - e^{-\beta\omega} (2\pi\sigma^2)^{1/2}} e^{-\omega^2/2\sigma^2} \times \left[1 + b_{\mathbf{K}} \left(\frac{\omega^4}{\sigma^4} - \frac{6\omega^2}{\sigma^2} + 3 \right) \right], \quad (4.4)$$

where

$$b_{\mathbf{K}} = \frac{\sigma^4 \langle \omega^4 \rangle_{\mathbf{K}}}{24 \langle \omega^0 \rangle_{\mathbf{K}}} - \frac{1}{8}, \quad (4.5)$$

$$\sigma^2 = \langle \omega^2 \rangle_{\mathbf{K}} / \langle \omega^0 \rangle_{\mathbf{K}}. \quad (4.6)$$

The Gram-Charlier representation results have been computed (again by using only the first two terms in the high-temperature expansion of the moments $\langle \omega^{2n} \rangle_{\mathbf{K}}$ for $n=0, 1, 2$) and are given as dashed curves in Figs. 1(d), 2(b), 2(d)–2(f), 2(h)–2(j), 2(m)–2(o), and 2(q)–2(t). Because for small \mathbf{K} values the Gram-Charlier series results are grossly inadequate, therefore they have not been plotted for $|\mathbf{K}| < 0.3 \text{ \AA}^{-1}$. For large \mathbf{K} values, the Gram-Charlier expansion gives relatively reasonable representation of the lineshape. Indeed, for many of the given plots the disagreement between the results of the two-parameter Gaussian approximation

and the Gram-Charlier series expansion is too small to be adequately displayed.

V. CONCLUDING REMARKS

The spectral line shape computed in the preceding section is found to be in acceptable agreement with the parameter-free experimental observation of $S(\mathbf{K}, \omega)$ in paramagnetic RbMnF_3 . The theoretical estimate of the line shape is subject to several possible uncertainties. These uncertainties fall roughly into two distinct categories: (a) those that arise because of the approximate nature of the system Hamiltonian (b) and those that are the result of approximations made in deriving the given theoretical expressions.

The approximations associated with the physical model being analyzed can be farther subdivided into two classes: To the first class belongs the assumption that the spin degrees of freedom are not coupled to the lattice degrees of freedom. The second class relates to the actual representation of the Hamiltonian dealing with the spin degrees of freedom and to any approximations that are thereby introduced.

The first of these assumptions ignores the possibility of magnetovibrational scattering. Realistic estimates of the inaccuracy caused by this assumption cannot be made. The hope, however, is that the major renormalization of the purely magnetic scattering results, i.e., due to the magnetovibrational effects, will be in the neighborhood of small frequencies. The measurement of $S(\mathbf{K}, \omega)$ for small frequencies is in any case subject to much uncertainty due to the presence of sizable amounts of elastic nuclear scattering.

The second of these assumptions deals with the use of isotropic, nearest neighbor Heisenberg exchange model. This assumption is perhaps the least serious because the low-temperature measurements of Windsor and Stevenson²⁸ clearly show that the nearest-neighbor exchange dominates. The neglect of the next-nearest-neighbor exchange should therefore cause uncertainties of only a few percent.

The second category of approximations dealing with the theoretical derivation of the spectral line shape involve the uncertainties associated with the assumption of a two-parameter Gaussian representation for the generalized diffusivity as well as with the calculation of the frequency moments $\langle \omega^{2n} \rangle_{\mathbf{K}}$, $n=0, 1$ and 2 (upon which the determination of the parameters of the diffusivity depends). As our previous studies¹⁷ have shown, the two-parameter Gaussian representation for the diffusivity is adequate for studying $S(\mathbf{K}, \omega)$ at elevated temperatures. Therefore, the major uncertainty in this category is probably caused by the approximate evaluation of the frequency moments themselves. As the SRO contributions to the fourth moment have only very crudely been estimated by keeping only the first finite-temperature correction (beyond the infinite temperature term), therefore the

given estimate for the fourth moment may be subject to possible errors of several percent. The zeroth and the second moment, on the other hand, are probably accurate to a few percent.

It is instructive to examine the experimental and the theoretical results for the spin diffusion. Windsor *et al.*²⁵ have used their small- \mathbf{K} results for $S(\mathbf{K}, \omega)$ and analyzed them in terms of the best-fitting Lorentzian line shapes, i.e.,

$$S(\mathbf{K}, \omega) = \frac{1}{\pi} \frac{S(S+1)DK^2}{\omega^2 + (DK^2)^2}. \quad (5.1)$$

They have given their results in the form of a plot of DK^2 against the average value of \mathbf{K} . (Here D is the spin-diffusion constant).

In Fig. 3 we have plotted our $D(\mathbf{K}, 0)$ against the average value of \mathbf{K} for infinite temperatures as well as for the temperature of interest. [Note that $D(\mathbf{K}, 0)$ should be the analogue of DK^2 for small \mathbf{K} .] The finite-temperature results for $D(\mathbf{K}, 0)$ were obtained in the following way: In the expression

$$D(\mathbf{K}, 0) = \frac{\sqrt{(\pi) \langle \omega^2 \rangle_{\mathbf{K}}^{3/2} / (2 \langle \omega^0 \rangle_{\mathbf{K}})^{1/2}}}{[\langle \omega^0 \rangle_{\mathbf{K}} \langle \omega^4 \rangle_{\mathbf{K}} - (\langle \omega^2 \rangle_{\mathbf{K}})^2]^{1/2}} \quad (5.2)$$

[compare with Eqs. (4.2) and (4.3)], we used the results for the moments, $\langle \omega^{2n} \rangle_{\mathbf{K}}$ correct only to the first two dominant powers in $\frac{1}{2}(\beta I)$. This procedure would seem to be somewhat wasteful in the sense that it does not make use of the most accurate expressions for $\langle \omega^0 \rangle_{\mathbf{K}}$ and $\langle \omega^2 \rangle_{\mathbf{K}}$, but it was adopted to get a feel for the maximum discrepancy that the theoretical results have with respect to the experimental results. The relative fit of the experimental results and the above theoretical estimates is seen to be within the limits of accuracy that would be placed on the result given in Eq. (5.2) because of the inaccuracy of the frequency moments (within the approximation whereby only the first finite-temperature correction is retained).

It is interesting to compare the experimental results for the magnitude of the spin diffusion D , i.e.,

$$D = \lim_{\mathbf{K} \rightarrow 0} [D(\mathbf{K}, 0)/K^2] \quad (5.3)$$

with those obtained from Eqs. (5.2) and (5.3). Using only the first temperature correction for the moments $\langle \omega^{2n} \rangle_{\mathbf{K}}$ in these equations we find

$$D = 1.60D(\infty). \quad (5.4)$$

On the other hand, if we use the more accurate calculations for $\langle \omega^0 \rangle_{\mathbf{K}}$ and $\langle \omega^2 \rangle_{\mathbf{K}}$ given in Eqs. (3.5) and (3.6), we find

$$D = 1.40D(\infty). \quad (5.5)$$

In Eqs. (5.4) and (5.5), $D(\infty)$ denotes the corresponding result for D in the infinite-temperature limit.

The experimental result for D obtained by Windsor *et al.* is quoted to be $= 8.0 \pm 1.0$ meV \AA^2 . It is convenient

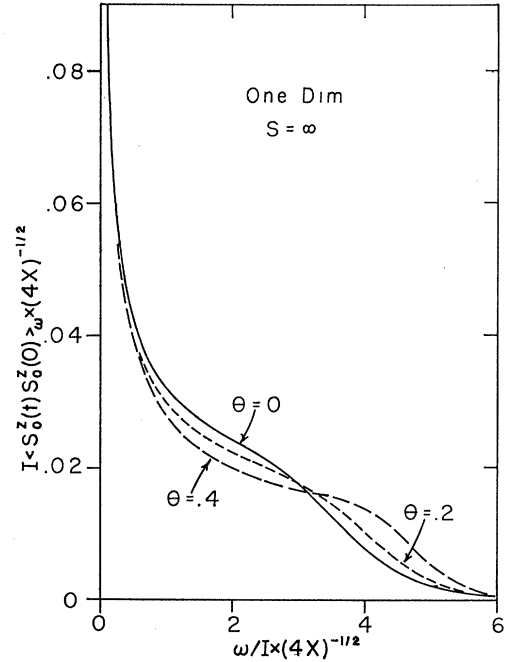


FIG. 4. Effect of finite temperature on frequency Fourier transform of the self-correlation function. The Fourier transform is plotted against the reduced frequency and refers to the linear chain with isotropic nearest-neighbor exchange and $S = \infty$. For the linear chain, $\theta = 4\beta IX$.

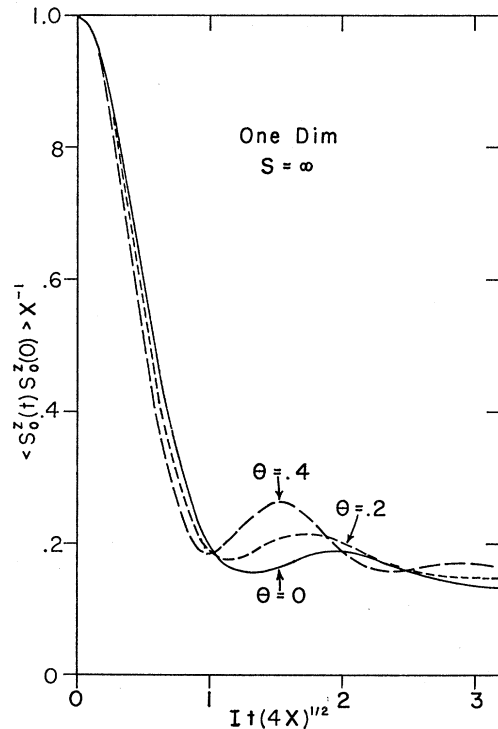


FIG. 5. Effect of finite temperature on the time-dependent self-correlation function for the linear chain with isotropic nearest-neighbor exchange and $S = \infty$. The ordinate is an appropriate Fourier transform of the corresponding curves in Fig. 4.

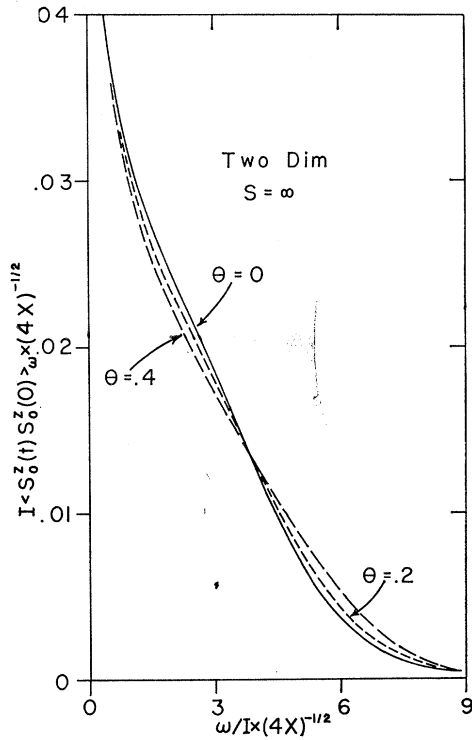


FIG. 6. Effect of finite temperature on frequency Fourier transform of the self-correlation function are displayed by plotting the Fourier transform against the reduced frequency. The plot refers to a two-dimensional square net with isotropic nearest-neighbor exchange and $S = \infty$. For the square net, $\theta = 8\beta IX$.

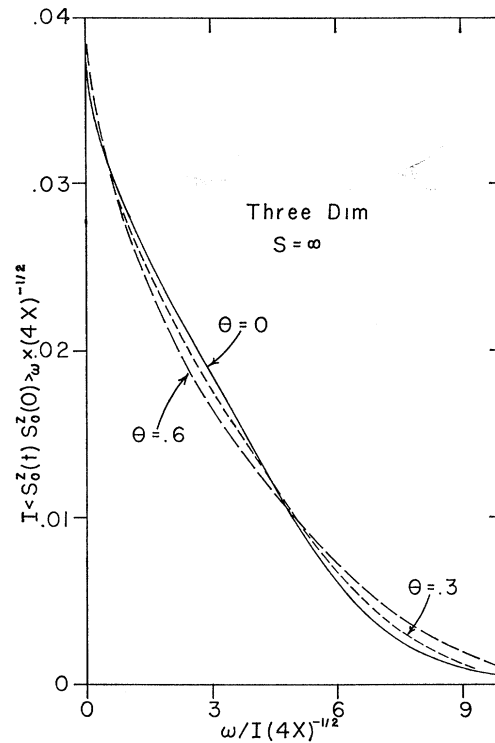


FIG. 7. Demonstration of the effect of finite temperature on frequency Fourier transform of the self-correlation function. The Fourier transform is plotted against the reduced frequency and refers to the simple cubic lattice with isotropic nearest-neighbor exchange and $S = \infty$. For the simple cubic lattice, $\theta = 12\beta IX$.

to transform to the dimensionless parameter Δ

$$\Delta(T) = D/2Ia_0^2(3X)^{1/2}, \quad (5.6)$$

where a_0 is the lattice constant of RbMnF_3 at room temperature [note that $a_0 \sim 4.34 \text{ \AA}$]. Our theoretical results for Δ , i.e.,

$$\Delta(T = 293^\circ\text{K}) = 0.360, \quad (5.7a)$$

$$\Delta(T = \infty) = 0.257, \quad (5.7b)$$

where we have used the most accurate values of the moments, should be compared with the experimental result

$$[\Delta(T)]_{\text{expt}} = 0.27 \pm 0.03. \quad (5.7c)$$

Considering the approximate nature of the finite temperature result for the frequency moments, the results (5.7a) and (5.7c) are in acceptable agreement.

It should be mentioned here that Huber³³ has recently used the sixth frequency moment, $\langle \omega^6 \rangle_{\mathbf{k}}$, given in Ref. 17 to make an estimate of the accuracy of the spin-diffusion constant as given by the two-parameter Gaussian approximation. His conclusion is that this procedure should lead to values for D which are within 10% of the correct value. In view of the fact that $\Delta(T)$ is subject to the above mentioned inaccuracies, the agreement

between the experiment and the theory is entirely acceptable.

In conclusion it should be mentioned that we have also computed the effects of SRO upon the time-dependent self-correlation function $\langle S_0^z(t) S_0^z(0) \rangle$ and its frequency Fourier transform. These results are obtained by using Eqs. (4.1)–(4.3). In order not to get involved with real and imaginary parts of the correlation $\langle S_0^z(t) S_0^z(0) \rangle$ we have plotted only the infinite (i.e., classical) spin results for which the imaginary part is vanishing.

A study of Figs. 4–7, where these results are plotted, reveals the evolution of the following interesting structure with the increase in the SRO (a measure of the SRO is the largeness of the value of θ). As the SRO increases, the Fourier transform $\langle S_0^z(t) S_0^z(0) \rangle_{\omega}$ begins to develop a hump. The prominence of this hump is found to be greater the lower the dimensionality.

ACKNOWLEDGMENTS

We are greatly indebted to the Temple University Computer Center for the use of their CDC 6400. Our thanks are also due Dr. C. G. Windsor for providing us his experimental data on RbMnF_3 and Professor D. L. Huber for sending his preprint on spin diffusion.

³³ See D. L. Huber (unpublished).